Marine Structures 28 (2012) 67–85

Contents lists available at SciVerse ScienceDirect

Marine Structures

journal homepage: www.elsevier.com/locate/marstruc

# Motion-based wave estimation: Small-scale tests with a crane-barge model

Eduardo A. Tannuri [a,*], Alexandre N. Simos [b], João V. Sparano [b], Vinícius L.F. Matos [c]

[a] Mechatronics Eng. Dept., Escola Politécnica, University of São Paulo, Av. Prof. Mello Moraes 2231, São Paulo 05508-900, Brazil
[b] Naval Arch. & Ocean Eng. Dept., Escola Politécnica, University of São Paulo, Av. Prof. Mello Moraes 2231, São Paulo 05508-900, Brazil
[c] Petrobras – Exploration and Production, Macaé, Rio de Janeiro, Brazil

ARTICLE INFO

*Article history:*
Received 3 June 2011
Received in revised form 28 January 2012
Accepted 5 May 2012

*Keywords:*
Directional wave spectrum
Motion-based estimation
Crane-barge
Experimental validation
Bayesian estimation

ABSTRACT

This paper provides additional validation to the problem of estimating wave spectra based on the first-order motions of a moored vessel. Prior investigations conducted by the authors have attested that even a large-volume ship, such as an FPSO unit, could be adopted for on-board estimation of the wave field. The obvious limitation of the methodology concerns filtering of high-frequency wave components, for which the vessel has no significant response. As a result, the estimation range is directly dependent on the characteristics of the vessel response. In order to extend this analysis, further small-scale tests were performed with a model of a pipe-laying crane-barge. When compared to the FPSO case, the results attest that a broader range of typical sea states can be accurately estimated, including crossed-sea states with low peak periods.



## 1. Introduction

Considerable research effort has been recently dedicated to evaluate whether good-quality wave estimations could be obtained from the record of vessels' motions. Most of the previous work is focused on the problem of ships with forward speed and a good perspective on the state-of-the-art of this problem may be found in references [1–8]. The present paper, on the other hand, deals with the possibility of estimating the directional wave spectrum from the motions recorded aboard a stationary vessel, such as, for example, an FPSO (Floating Production Storage and Offloading) unit or a pipe-laying

* Corresponding author. Tel.: +55 1183545679; fax: +55 1130915414.
*E-mail address:* eduat@usp.br (E.A. Tannuri).

0951-8339/$ – see front matter © 2012 Elsevier Ltd. All rights reserved.
doi:10.1016/j.marstruc.2012.05.002

barge. The problem is obviously quite similar to the one based on a ship that moves forward, except for the well-known fact that the forward speed introduces a problem when dealing with following waves, as addressed in [2]. Another advantage of stationary units is that their headings usually changes very slowly along a typical acquisition interval (10–20 min), thus making the estimations easier.

When compared to other wave monitoring systems, such as buoys or radar systems, the main advantage that arises from this method concerns the simplicity of the instrumentation (composed basically of accelerometers and rate-gyros), which is very easy to install on-board and, furthermore, requires a rather uncomplicated maintenance, especially if compared to the wave-buoys. On the other hand, the limitation is also clear: only waves that impose a reasonable level of motions may be inferred. In other words, the vessel acts as a low-pass filter, filtering the high-frequency components that do not excite the vessel's first-order response. That is the main reason why this kind of methodology cannot be envisaged as a substitute for wave-buoys for the sake of long-term oceanographic records. It may, however, provide important information concerning the operation of such vessels when the problems are directly connected to the waves in the range of frequencies that do impose significant motions of the floating unit.

The filter analogy also indicates that the range of frequencies for which the spectrum can be estimated will depend decisively on the size of the vessel. Large-displacement vessels, such as the VLCCs on which the FPSOs are usually based, will have lower *cut-off* frequencies if compared to smaller vessels, such as a crane-barge.

The present paper is part of a research project that has been conducted at the University of São Paulo and which is sponsored by Petrobras. The main objective is to develop a wave monitoring system that may be installed on-board production units operating in the deep-water areas of Campos Basin in Brazil and also on service boats, such as the pipe-laying crane-barges that Petrobras operates. Previous results obtained in this context were already published. In Ref. [10], the performance of an FPSO as a "wave sensor" was first analyzed based exclusively on numerical simulations. This work also addressed an important issue, almost constantly overlooked in the literature on this subject: the sensibility of the response concerning possible errors on the transfer functions of motions (the RAOs). Such errors may arise from the inertial parameters, which depend on the vessel loading (critical in the case of FPSOs) and also due to non-linear effects on the response. This latter aspect is especially important when dealing with the roll motions, which are usually resonant and strongly dependent on the viscous damping of the hull. Although most of the previous work on the subject proposed dealing with the classical heave-pitch-roll motions (probably induced by a direct analogy to the wave-buoys), this is not the only option, as the whole set of motions in 6 d.o.f. encompasses redundant information on the wave direction. For this reason, it was previously proposed that the roll motion should be replaced by the sway motion, in order to increase the reliability of the estimations (see Ref. [10]). On a second phase of the research project, some field data was provided by Petrobras, regarding a monitoring campaign of one of its FPSOs. Waves estimated from the motion records were compared to those provided by a wave-buoy installed nearby and the results were presented in [11]. Although good results could be obtained, problems with the wave-buoy restricted the analysis to a few cases, certainly not enough for a substantial full-scale validation. The analysis was then complemented by model tests conducted in LabOceano's ocean basin in Brazil. In a first stage, the model of the same FPSO that provided the real-scale data was tested. Model scale was 1:70 and the results obtained in this campaign were presented and discussed in Ref. [12].

Experimental validation was later completed by testing a 1:48 scale model of a crane-barge (BGL-1). These tests were conducted at the same ocean basin and included the emulation of long-crested and short-crested seas with different levels of directional wave spreading, and also crossed-sea states. The assessment of the accuracy of wave predictions derived from the motions of the crane-barge model is then the main goal of the present paper.

Next section presents a description of the small-scale tests conducted at the ocean basin, providing data on the model and the sea conditions and also describing the instrumentation employed. This is followed by a presentation of the method adopted for the wave inference, based on a Bayesian approach. Finally, the wave estimations obtained by this method using as input the motions recorded in the tests are directly compared to wave spectra measured in the basin by means of an array of wave probes.

## 2. Experimental procedure

The Petrobras' pipe-laying crane-barge BGL-1 has a 120 m-long hull, with almost square sections. A picture of hers during operation can be seen in Fig. 1, together with a view of her small-scale model. The model was built in 1:48 scale. The vessel main dimensions are presented in Table 1, in both real and model scales. The LCG is related to the midship section.

Model tests were carried out in LabOceano, Rio de Janeiro. The facility includes an ocean basin which is 45 m long, 30 m wide, 15 m deep equipped with multi-directional wave generation. The wave generation system is based on an array of 75 flap-type wavemakers that allow emulating short-crested seas with variable spreading, as well as crossed-sea conditions, by the combination of two different long-crested seas with different directions. Fig. 2 shows a sketch of the LabOceano basin and the two coordinate systems adopted for the analysis. Directional wave spectra will be presented in two different patterns: in a polar plot relative to a vessel local reference frame (180° denoting bow incidence) and also in the basin-fixed reference frame (0° denoting waves that propagate perpendicular to the wavemakers, toward the opposite beach).

The model was kept in position by means of a soft mooring system consisting of four low-stiffness springs mounted horizontally in air. The only purpose of the system was to keep the models offsets within the limits required by the optical monitoring system, having no influence on the model's wave-frequency motions.

Wave calibration tests were performed in the absence of the model and the evaluation of the directional wave spectrum within the test zone was performed by means of a wave probe array (the methodology adopted by LabOceano for estimating the directional wave spectra follows closely Stansberg [14]; a detailed description of the wave calibration procedure was given by Tannuri et al. [15]). The set of wave spectra obtained in the calibration tests was later used for validation purposes.

Irregular wave tests were performed for intervals corresponding to 3 h in real-scale, during which the motions of the vessel in 6 d.o.f. were measured by means of an optical device. This measurement system already outputs the CG position and orientation angles of the model, with respect to which the RAOs were derived (details on the estimation procedure will be given in the next section). The complete set of waves that were tested is listed in Table 2 (all values in real-scale). The JONSWAP.

10-parameter model used to define general bimodal ($i = 1,2$) wave spectrum is given by:

$$S(\omega,\theta) = \frac{1}{4}\sum_{i=1}^{2} 2\pi\alpha_i \frac{g^2}{\omega^5} A(s_i)\cos^{2s_1}\left(\frac{\theta-\theta_{m_1}}{2}\right)\exp\left[\frac{-1.25\omega_{p_1}^4}{\omega^4}\right]\gamma_i^{\exp}\left[-\frac{-(\omega-\omega_{p_i})^2}{2\sigma_i^2\omega_{p_i}^2}\right] \quad (1)$$

where $g$ is the gravity acceleration, $\omega_p$ is the peak frequency ($\omega_p = 2\pi/T_p$; $T_p$ is the peak period), $s$ is the spreading factor. The peakedness parameter $\gamma$ is a shape factor and $\sigma$ is the peak width, given by 0.07 (if $\omega \leq \omega_p$) or 0.09 (if $\omega > \omega_p$). The term $\alpha$ is related to the significant height $H_s$, and to the peak frequency by:

$$\alpha = 5.0609\frac{H_s^2\omega_p^4}{(2\pi)^4}(1 - 0.0287\ln\gamma)$$

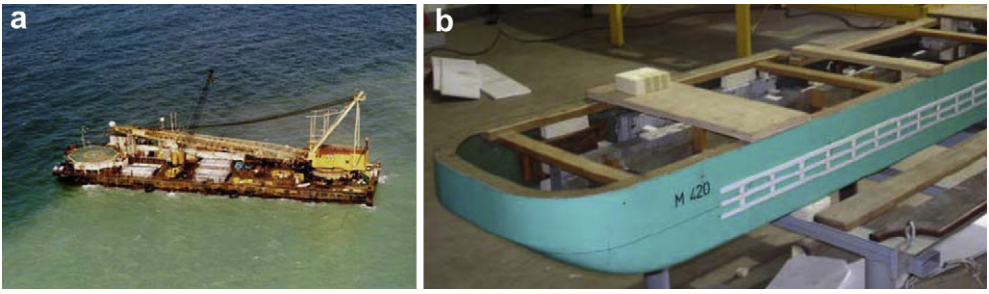


**Fig. 1.** Pictures of the Petrobras' BGL-1 crane-barge and her small-scale model.

**Table 1**
BGL main dimensions.

| Dimensions | Real scale | Model scale (1:48) |
|---|---|---|
| L (m) | 120 | 2.5 |
| B (m) | 30.48 | 0.64 |
| D (m) | 8.53 | 0.18 |
| T (m) | 5 | 0.104 |
| Disp. (tons) | 1.75E + 04 | 0.158 |
| LCG (m) | 1.265 | 0.026 |
| TCG (m) | 0 | 0 |
| VCG (m) | 4.83 | 0.101 |
| Ixx (ton*m$^2$) | 2.60E + 06 | 1.02E − 02 |
| Iyy (ton*m$^2$) | 1.57E + 07 | 6.17E − 02 |
| Izz (ton*m$^2$) | 1.57E + 07 | 6.17E − 02 |

Function $A(s)$ is a normalization factor, given by:

$$A(s) = \frac{2^{2s-1}\Gamma^2(s+1)}{\pi\Gamma(2s+1)}$$

The tested waves can be subdivided in four main groups of tests, as explained next: The first group of experiments (BGL90IX) corresponds to beam-sea (incidence of 90° with respect to the vessel local coordinate system) conditions with unimodal (single-peaked) energy spectra. Tests denoted by $X = 1,3,4$ have the same height and period, but increasing directional spreading. Values of height and period correspond to a typical 1 year-return condition, according to Campos Basin metocean data. Test $X = 2$ represents the most severe 100yr condition estimated for Campos Basin. The same pattern is adopted in the third group of experiments (BGL135IX), which is equivalent to the first set, but now with an incidence angle of 135° with respect to the vessel coordinate system.

The spreading factor adopted for the tests denoted by $X = 1,3,4$ were selected in order to test the performance of the method in face of waves with very different directional spreading, while keeping the other parameters unchanged. To capture the effects more properly, a wide spreading range was chosen, varying from long-crested wave (in tests I1, $s = \infty$) to a relatively large spreading ($s = 12$). Goda [16] indicates a value around $s = 10$ to be representative of wind waves, while typical values for swell seas would vary from $s = 25$ (swell with relatively large steepness) to $s = 75$ (with relatively small wave

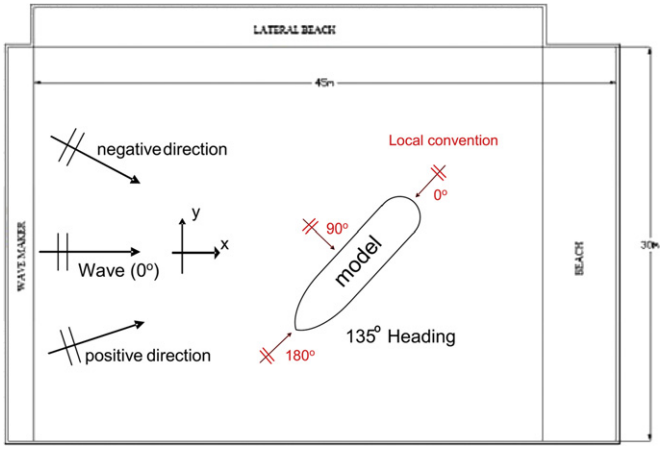


**Fig. 2.** LabOceano basin. Global (black) and Local (red) reference systems for wave direction. (For interpretation of the references to colour in this figure legend, the reader is referred to the web version of this article.)

**Table 2**
Set of waves for experimental tests at LabOceano – theoretical values.

| *Test* | Type | Wave parameters | | | | |
|---|---|---|---|---|---|---|
| | | Hs (m) | Tp (s) | Spreading factor s | Peakedness factor $\gamma$[a] | Direction (deg)[b] |
| BGL90I1 | Irregular | 4.59 | 10.12 | Infin. | 1.51 | 0 |
| BGL90I2 | | 8.05 | 14.56 | Infin. | 1.70 | 0 |
| BGL90I3 | | 4.67 | 10.12 | 60 | 1.51 | 0 |
| BGL90I4 | | 4.63 | 10.12 | 12 | 1.51 | 0 |
| BGL120B1 | Bimodal | 1.49(1) 1.00(2) 1.80(A) | 11.57(1) 6.65(2) 11.57(A) | – | 1.4(1) 0.9(2) | −30(1) 30(2) |
| BGL120B2 | | 2.02(1) 0.72(2) 2.14(A) | 7.34(1) 9.28(2) 7.34(A) | – | 1.6(1) 2.0(2) | −30(1) 15(2) |
| BGL120B3 | | 1.49(1) 0.62(2) 1.61(A) | 5.33(1) 11.29(2) 11.29(A) | – | 1.3(1) 2.2(2) | −30(1) 30(2) |
| BGL120B4 | | 2.02(1) 1.01(2) 2.25(A) | 11.43(1) 11.43(2) 11.43(A) | – | 1.5(1) 1.2(2) | −30(1) 30(2) |
| BGL120B5 | | 1.49(1) 1.00(2) 1.80(A) | 11.57(1) 6.65(2) 11.57(A) | – | 1.4(1) 0.9(2) | −30(1) −30(2) |
| BGL135I1 | Irregular | 4.59 | 10.12 | Infin. | 1.51 | 0 |
| BGL135I2 | | 8.05 | 14.56 | Infin. | 1.70 | 0 |
| BGL135I3 | | 4.67 | 10.12 | 60 | 1.51 | 0 |
| BGL135I4 | | 4.63 | 10.12 | 12 | 1.51 | 0 |
| BGL150B1 | Bimodal | 1.49(1) 1.00(2) 1.80(A) | 11.57(1) 6.65(2) 11.57(A) | – | 1.4(1) 0.9(2) | −30(1) 30(2) |
| BGL150B2 | | 2.02(1) 0.72(2) 2.14(A) | 7.34(1) 9.28(2) 7.34(A) | – | 1.6(1) 2.0(2) | −30(1) 15(2) |
| BGL150B3 | | 1.49(1) 0.62(2) 1.61(A) | 5.33(1) 11.29(2) 11.29(A) | – | 1.3(1) 2.2(2) | −30(1) 30(2) |
| BGL150B4 | | 2.02(1) 1.01(2) 2.25(A) | 11.43(1) 11.43(2) 11.43(A) | – | 1.5(1) 1.2(2) | −30(1) 30(2) |
| BGL150B5 | | 1.49(1) 1.00(2) 1.80(A) | 11.57(1) 6.65(2) 11.57(A) | – | 1.4(1) 0.9(2) | −30(1) −30(2) |

[a] Here we assume a JONSWAP spectrum type.
[b] Global (tank) coordinate system.

steepness). Thus, the values in the tests were chosen to represent the spreading for wind waves ($s = 12$) and swell ($s = 60$), while keeping the height and peak period constant.

The second group of experiments in Table 2, labeled BGL120BX, consists of crossed-sea sea conditions with bimodal energy spectra. The vessel heading for these tests corresponds to 120° with respect to the basin coordinate system. These waves were generated by combining two long-crested seas with different heights, periods and directions. In these cases, the data in Table 2 specifies $H_s$ and $T_p$ for both components (indicated by the numbers (1) and (2)) and also their average (combined) values ($A$), as derived from the analysis of the calibration tests. The angle between wave directions is 60° (+30° and −30° in the basin-fixed coordinate system) for the tests $X = 1,3,4$ and 45° for $X = 2$. The test $X = 5$ combines two wave components with different peak periods, but coming from the same direction. Finally, the fourth group (BGL150BX) consists of tests with the same waves of the second group, but now with a vessel heading of 150° in the basin coordinate system.

Next, the methodology adopted for motion-based estimations will be presented.

## 3. Wave inference method

Wave spectrum is estimated from the recorded vessel motions by means of a Bayesian inference method, originally proposed by Iseki & Ohtsu [2] and later refined by Nielsen [8]. The method that is employed in this paper follows closely the one proposed by Nielsen, except for the set of motions that is adopted as input for the estimations: as explained in the introduction, the roll motion is disregarded here due to the strong nonlinearities that affect the transfer function of this motion with respect to the incident waves. The motions in the other 5 d.o.f. (surge, sway, heave, pitch and yaw) set the basis for the estimations discussed ahead.

The Bayesian estimation is based on the maximization of the product between the maximum likelihood function and a prior distribution, which represents the previous information regarding the unknown coefficients (in our case, the directional wave spectrum). The way that Bayes' theorem is applied in order to provide a useful mathematical algorithm for the motion-based wave estimation is well documented in literature and therefore will not be addressed here. The reader can find details on this subject, for example, in [2,3,6,8,11].

Ultimately, the inference method requires the minimization of the following functional:

$$J(\mathbf{x}) = |\mathbf{B} - \mathbf{A}\mathbf{x}|^2 + \mathbf{x}^T\left(u_1^2\mathbf{H}_1 + u_2^2\mathbf{H}_2 + u_3^2\mathbf{H}_3\right)\mathbf{x} \tag{2}$$

In the expression above, $\mathbf{x}$ is the vector containing the unknown spectrum values for different wave frequencies$(\omega_m, m = 1, ..., M)$ and directions $(\theta_k, k = 1, ..., K)$:

$$\mathbf{x} = \begin{bmatrix} S(\omega_1,\theta_1) \\ S(\omega_1,\theta_2) \\ \vdots \\ S(\omega_M,\theta_{K-1}) \\ S(\omega_M,\theta_K) \end{bmatrix}$$

The vector $\mathbf{B}$ contains the values of the motion spectrum $\varphi_{ii}(\omega_m)$ and cross-spectrum $\varphi_{ij}(\omega_m)$ for the $N$ different motions that are used as input (in this paper then, $N = 5$). $\mathbf{B}$ is given by:

$$\mathbf{B} = [\,\mathbf{b}_1 \quad \mathbf{b}_2 \quad ... \quad \mathbf{b}_M\,]^T, with\ \mathbf{b}_m = \begin{bmatrix} \varphi_{ii}(\omega_m) \\ \vdots \\ \mathrm{Re}[\varphi_{ij}(\omega_m)] \\ \vdots \\ \mathrm{Im}[\varphi_{ij}(\omega_m)] \\ \vdots \end{bmatrix} \tag{3}$$

Welch's method was used for the estimation of power and cross-spectra of motions from their time series. Each motion record was divided into eight sections with 50% overlap, each section being filtered by a Hanning window.

$\mathbf{A}$ is the $(N^2 \cdot M) \times (K \cdot M)$ matrix that contains the dynamic characteristics of the vessel, expressed by means of its linear transfer functions of motion or RAOs. It can thus be written as:

$$\mathbf{A} = \begin{bmatrix} \mathbf{A}_1 & \mathbf{0} & \cdots & \mathbf{0} \\ \mathbf{0} & \mathbf{A}_2 & \cdots & \mathbf{0} \\ \vdots & \vdots & \ddots & \\ \mathbf{0} & \mathbf{0} & & \mathbf{A_M} \end{bmatrix} \tag{4}$$

with $\mathbf{0}$ the $N^2 \times K$ **zero** matrix and

$$\mathbf{A}_m = \begin{bmatrix} |RAO_i(\omega_m,\theta_1)|^2 & \cdots & |RAO_i(\omega_m,\theta_k)|^2 & \cdots & |RAO_i(\omega_m,\theta_K)|^2 \\ \mathrm{Re}\left(RAO_i(\omega_m,\theta_1)RAO_j(\omega_m,\theta_1)^*\right) & \cdots & \mathrm{Re}\left(RAO_i(\omega_m,\theta_k)RAO_j(\omega_m,\theta_k)^*\right) & \cdots & \mathrm{Re}\left(RAO_i(\omega_m,\theta_1)RAO_j(\omega_m,\theta_K)^*\right) \\ \mathrm{Im}\left(RAO_i(\omega_m,\theta_1)RAO_j(\omega_m,\theta_1)^*\right) & \cdots & \mathrm{Im}\left(RAO_i(\omega_m,\theta_k)RAO_j(\omega_m,\theta_k)^*\right) & \cdots & \mathrm{Im}\left(RAO_i(\omega_m,\theta_1)RAO_j(\omega_m,\theta_K)^*\right) \\ \vdots & & \vdots & & \vdots \end{bmatrix}$$

The second term in equation (2) allows one to predefine different levels of smoothness of the estimated spectrum regarding its variation in frequency and direction and also avoids predicting spurious wave energy for frequencies outside the range of wave frequencies for which the vessel presents significant response.

Smoothness is controlled by means of the so-called hyperparameters $\{u_1, u_2\}$, in a way that can be easily understood: Assuming that the spectrum is smooth with respect to direction and frequency and defining the second order differences $\varepsilon_{1mk}$ associated to direction $k$ at frequency $m$ and $\varepsilon_{2mk}$ associated to the frequency $m$ at the direction $k$ as:

$$\begin{aligned} \varepsilon_{1mk} &= S(\omega_m,\theta_{k-1}) - 2S(\omega_m,\theta_k) + S(\omega_m,\theta_{k+1}) \\ \varepsilon_{2mk} &= S(\omega_{m-1},\theta_k) - 2S(\omega_m,\theta_k) + S(\omega_{m+1},\theta_k) \end{aligned} \tag{5}$$

the smoothness condition is equivalent to keeping the following summations as small as possible:

$$\sum_{k=1}^{K}\sum_{m=1}^{M}\varepsilon_{1mk}^{2} = \mathbf{x}^{\mathbf{T}}\mathbf{H}_1\mathbf{x} \text{ with } S(\omega_m,\theta_0) = S(\omega_m,\theta_K) \text{ and } S(\omega_m,\theta_{K+1}) = S(\omega_m,\theta_1) \tag{6}$$

$$\sum_{k=1}^{K}\sum_{m=2}^{M-1}\varepsilon_{2mk}^{2} = \mathbf{x}^{\mathbf{T}}\mathbf{H}_1\mathbf{x}$$

where the matrixes $\mathbf{H}_1$ and $\mathbf{H}_2$ may be easily constructed considering the proper definition of the vector $\mathbf{x}$ (see, for example Ref. [8],). Thus, the hyperparameters $\{u_1, u_2\}$ operate in order to preset the level of smoothness desired in direction and frequency, respectively.

Furthermore, in order to avoid excessive spectral energy at the frequency boundaries, a third parameter is introduced. The reason why this is indeed necessary is clear: if the vessel has no significant response for a given wave-frequency, then any amount of wave energy could be predicted in this range. In order to guarantee that this aspect has no significant influence on the estimated spectrum, the sum of the power of the spectrum is minimized in a pre-defined range of low and high frequencies given by $(\omega_1, \omega_2, ..., \omega_L, \omega_H, ..., \omega_M)$. Considering the discretization presented above, the following functional must be minimized (matrix $\mathbf{H}_3$ is obtained by a procedure similar to the one used to derive $\mathbf{H}_1$ and $\mathbf{H}_2$):

$$\sum_{k=1}^{K}\sum_{m=1}^{L} S(\omega_m,\theta_k)^2 + \sum_{k=1}^{K}\sum_{m=H}^{M} S(\omega_m,\theta_k)^2 = \mathbf{x}^{\mathbf{T}}\mathbf{H}_3\mathbf{x} \tag{7}$$

The problem that arises then is that the three external parameters must be pre-defined and, in principle, their values may change with the vessel characteristics (hull geometry, draft, inertial parameters, etc.) and also with respect to the incoming wave features (wave height, peak period, angle of incidence, etc.), which, of course, are unknown. The calibration of the Bayesian inference model was subject of discussion in several articles. Iseki [3] and Nielsen [8], for example, proposed that optimum values of the hyperparameters should be estimated for each wave prediction according to the criterion originally introduced by Akaike [13]. Nielsen [5] describes in details how the so-called ABIC criterion can be numerically implemented in the context of motion-based wave estimation. The critical problem in this approach is that the application of ABIC requires a large number of computations, rendering the inference extremely time-consuming and, consequently, impractical for real-time on-board wave estimation. Nevertheless, previous studies based on an extensive set of tests performed in a wave basin with a small-scale model of a typical FPSO hull (see Ref. [12]) have shown that the estimations are quite insensitive to fluctuations of the hyperparameters. Therefore, Simos et al. [10] have adopted a different approach: the set of parameters were obtained through a previous calibration analysis of the hull, and a set of adequate (yet certainly not *optimum*) values was defined for various drafts of the vessel. This was done with the help of the ABIC criterion and numerical simulations of typical (frequent) wave conditions. The estimations were then performed with a fixed set of $\{u_1,u_2,u_3\}$, thus irrespective to the incoming wave features. This procedure that can be understood as a pre-calibration of the inference system was later studied by Nielsen & Iseki [9] concerning the problem of a ship with forward speed, reaching similar conclusions.

For that reason, for all the comparisons presented next, a pre-calibration of the BGL barge was conducted and a fixed set of hyperparameters was employed: $\{u_1 = 0.035, u_2 = 0.035, u_3 = 1.5\}$. Also, for avoiding spurious energy outside the range of frequencies with hull response (see eq. (7)), the following limits were adopted: $\omega_L = 0.31$ rad/s and $\omega_H = 1.26$ rad/s (values in real-scale, equivalent to wave periods of 20 s and 5 s, respectively). The RAOs of the barge, shown in Fig. 3, confirm the small motion response for wave periods below 5 s. The RAOs were obtained using a well-known wave–body interaction BEM code (WAMIT® [17]). Based on the model's hull geometry, numerical meshes were constructed considering the typical loading condition of the barge.

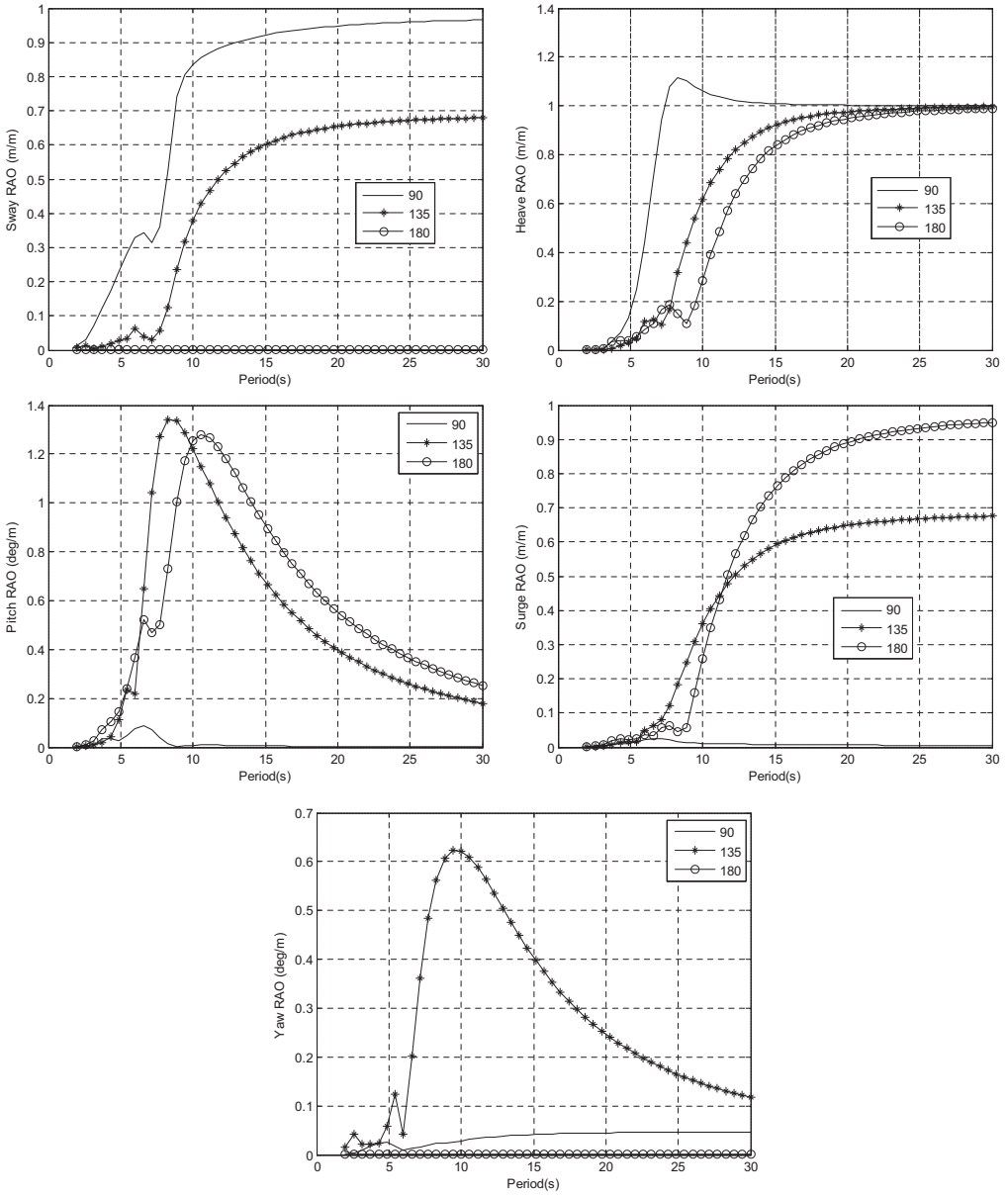


**Fig. 3.** BGL1 RAOs for 3 relative wave incidences (90°, 135° and 180°).

The mooring arrangement used in the tests induces yaw low-frequency oscillations at periods of 30 s or more, what justifies the value of $\omega_L$ adopted.

The number of directions ($K$) and frequencies ($M$) define the total size of the optimization problem, since the number of variables is K·M. In the present work, $K = 18$ (20° intervals with respect to wave direction) and $M = 25$ (considering a regular discretization in period, between 2 s and 30 s).

Next section discusses how statistical wave parameters estimated from model motions compare to the reference values of Table 3, for each wave condition. Different aspects of the estimation model, such as filtering of high-frequency components, are discussed based on illustrative results.

**Table 3**
Experimental results of the Bayesian estimation – unimodal waves – main statistical parameters.

| Case | Wave-probe estimation | | | Motion-based estimation | | | Errors | | |
|---|---|---|---|---|---|---|---|---|---|
| | $H_s$ (m) | $T_p$ (s) | Dir (deg) | $H_s$ (m) | $T_p$ (s) | Dir (deg) | $H_s$ (%) | $T_p$ (%) | Dir (deg) |
| BGL90I1 | 4.34 | 10.88 | −0.1 | 4.26 | 10.17 | 4.4 | −1.9 | −6.5 | 4.6 |
| BGL90I3 | 4.63 | 9.87 | 0.7 | 4.78 | 10.17 | 3.7 | 3.3 | 3.0 | 3.0 |
| BGL90I4 | 4.54 | 10.32 | 2.5 | 4.59 | 10.17 | 5.7 | 1.2 | −1.5 | 3.2 |
| BGL90I2 | 8.04 | 15.49 | 1.1 | 7.99 | 16.00 | 3.4 | −0.7 | 3.3 | 2.4 |
| BGL135I1 | 4.34 | 10.88 | −0.1 | 4.45 | 10.17 | −3.8 | 2.5 | −6.5 | −3.7 |
| BGL135I3 | 4.63 | 9.87 | 0.7 | 4.34 | 11.33 | −6.6 | −6.2 | 14.8 | −7.3 |
| BGL135I4 | 4.54 | 10.32 | 2.5 | 4.28 | 10.17 | −6.0 | −5.8 | −1.5 | −8.5 |
| BGL135I2 | 8.04 | 15.49 | 1.1 | 8.19 | 16.00 | −0.6 | 1.9 | 3.3 | −1.6 |

## 4. Comparison of motions-based and probes-based wave spectra

### 4.1. Unimodal waves

Several unimodal waves were considered, for 90° and 135° relative heading angles (cases BGL90IX and BGL135IX). Results indeed indicate an overall good agreement between Bayesian motion-based estimated spectra and those obtained from the wave probes measurements. Mean errors in the statistical parameters for all tests are shown in Table 3. The errors are defined as the difference between motion-based and wave-probe estimation. The maximum errors observed in $H_S$, $T_P$ and direction were 6.2%, 14.8% and 8.5°, respectively. The errors are smaller for beam-sea condition, compared to the 135° incidence tests. For beam-sea tests, only sway and heave motions are strongly excited by the waves, whereas for 135° incidence tests motions in the 5 d.o.f. are important. It is therefore expected that wave estimation will be more susceptible to inaccuracies in the model in the second case.

Besides the statistical parameters, the motion-based estimation can predict the shape of the wave spectrum with quite reasonable accuracy. Fig. 4 contains the radar plot of the estimated spectra by the motion-based method, considering both the 135° and 90° relative incidence angle for the tests I1, I3 and I4. The spectra obtained with the wave-probe array are also presented. In these figures, the circles represent the wave period. The wave spectra are presented in a different format in Fig. 5. Here, the spectrum maps are depicted in the wave tank reference system (mean wave direction is zero degrees in this case, as in Fig. 2). All plots share the same gray scale bar, since the interval of contour lines is the same in every case.

The growth in angular spreading from tests I1 to I3 and I4 can be visually inferred, and this is defined by the spreading factor $s$ (a more detailed discussion on this factor will be presented later). The shape of the directional spectra are quite similar for both, motion-based and wave-probe estimations.

Fig. 6 contains the power spectra derived from the motion-based estimations, compared to those obtained from the wave-probes. Again, the shape of the curves is very well predicted (this shape is dependent on the peakedness factor $\gamma$ considered in the generation of the JONSWAP spectra – see Table 2).

Finally, Fig. 7 presents the results of the 100-yr unimodal wave (BGLXXI2 tests). Since this wave presents energy in a low-frequency range, the effect of definition of the cut-off frequency $\omega_L = 0.31$ rad/s can be verified. In fact, for wave periods larger than 20 s, the Bayesian Method tends to reduce the estimated spectrum, as can be verified in the power spectrum plots. However, it does not degrades the spectrum and statistics estimation (the significant wave height, for example, presents 1.9% maximum error only).

A quantitative comparison concerning the shape factors ($s$ and $\gamma$) of the estimated spectra is presented in Table 4. This table contains, in its first part, the values that were specified to the wave-generator control software ("Specification"). Due to limitations in the generation process, the actual wave is slightly different from the specification (see, for example [15],). A function-fitting algorithm is then used to obtain the actual shape factors of the directional spectrum estimated with the

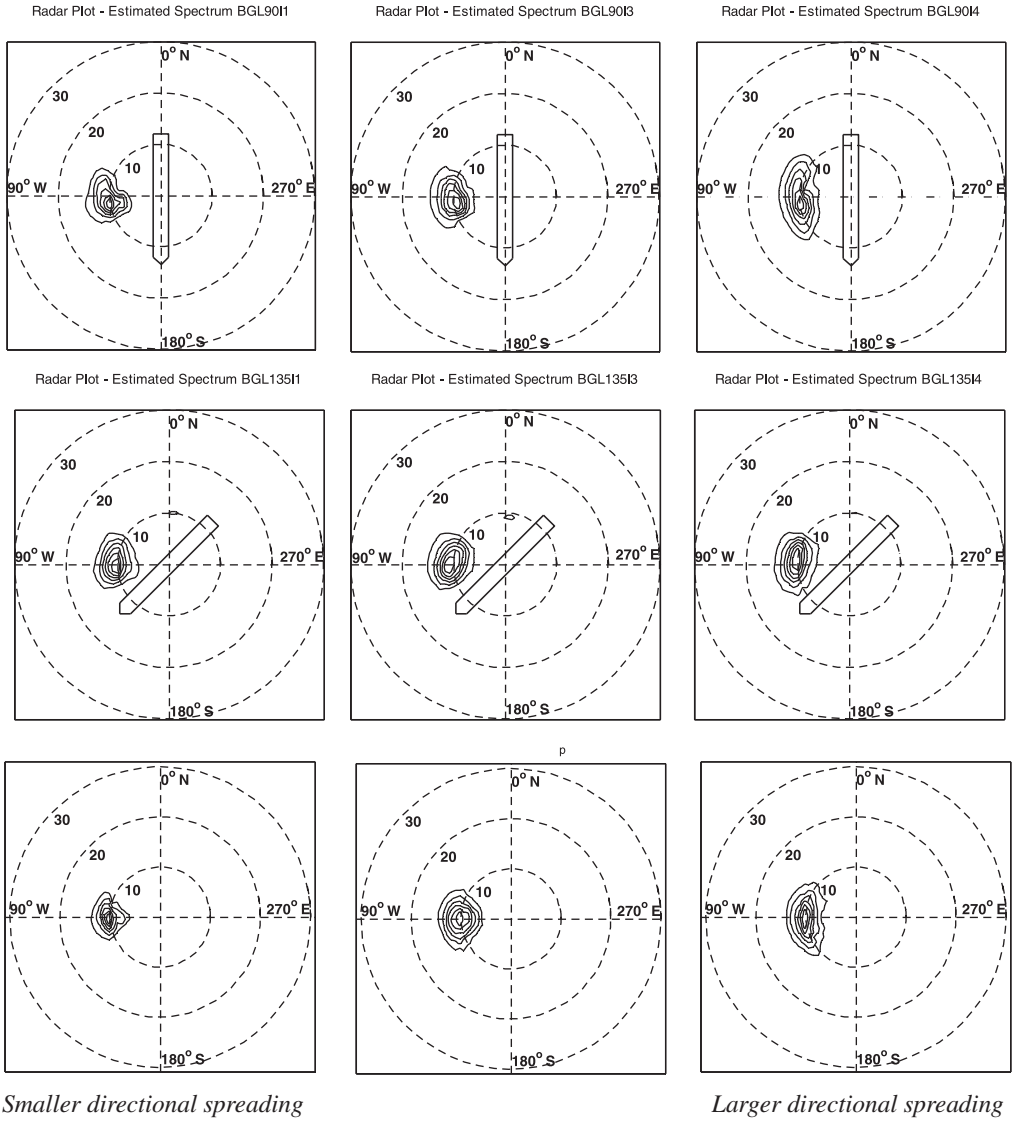


**Fig. 4.** Radar plot of estimated spectrum - unimodal waves with increasing directional spreading: (up) 90° incidence angle; (middle) 135° incidence angle; (down) Experimental Spectrum estimated by wave-probe array.

wave-probes (considered herein as the paradigm for comparisons). The same function-fitting algorithm is applied to the motion-based Bayesian estimated spectrum.

This algorithm is based on the definition of the JONSWAP spectrum (eq. (1)). A non-linear optimization routine is performed to find values of the 10 sea-parameters that minimizes the error between the estimated and the JONSWAP spectra.

For example, the spreading parameter for the test BGL90I4 is 12, for the BGL135I4 is 23 and the wave-probe estimation is 13. In fact, in the last column of Fig. 5 one can verify that, in fact, the BGL90I4 estimation is slightly more spread than the wave-probe estimation, whereas the one for BGL135I4 is slightly narrower.

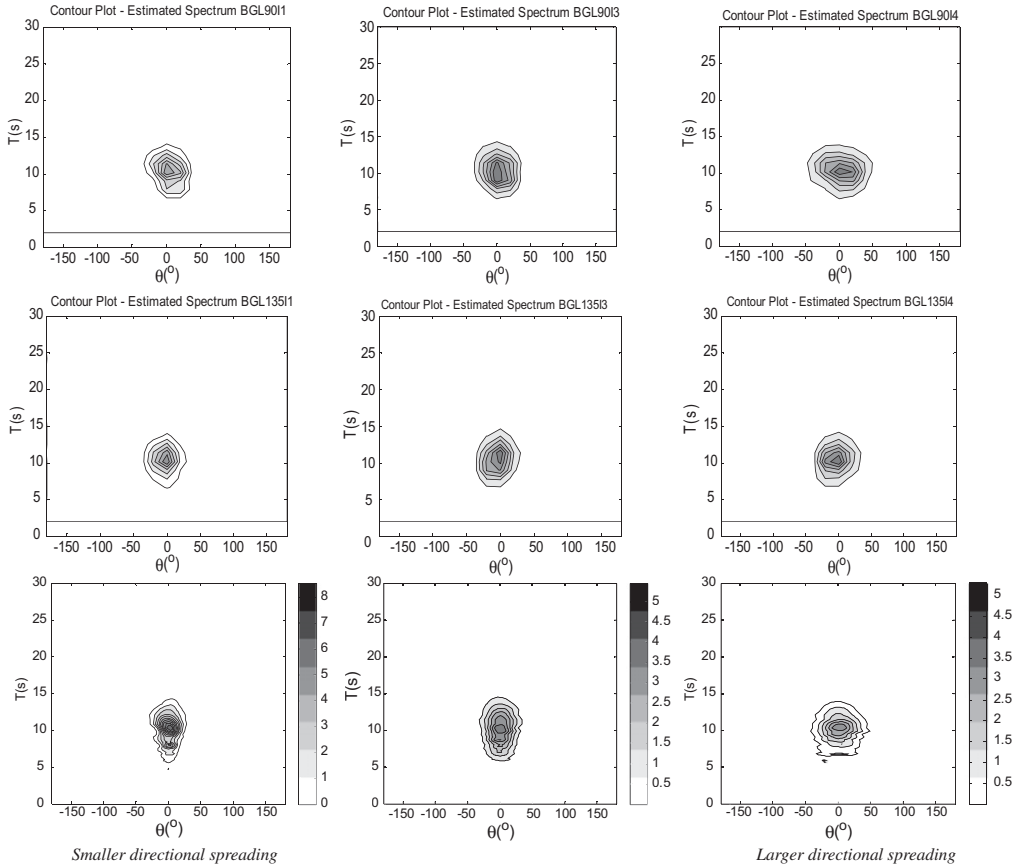


**Fig. 5.** Contour plot of directional spectrum - unimodal waves with increasing directional spreading: (up) 90° incidence angle; (middle) 135° incidence angle; (down) Experimental spectrum estimated by wave-probe array.

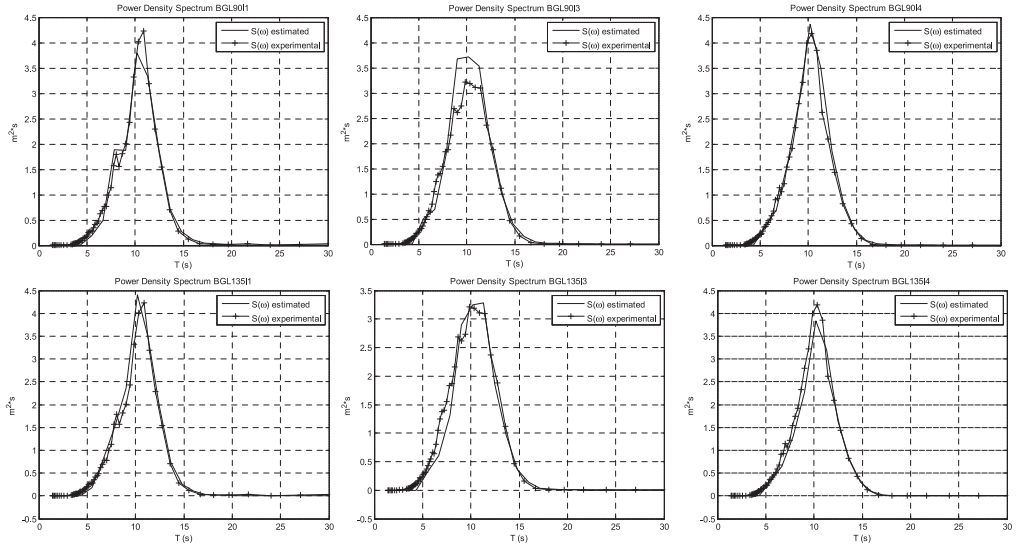


**Fig. 6.** Power density spectrum - unimodal waves with increasing directional spreading: (up) 90° incidence angle; (down) 135° incidence angle.

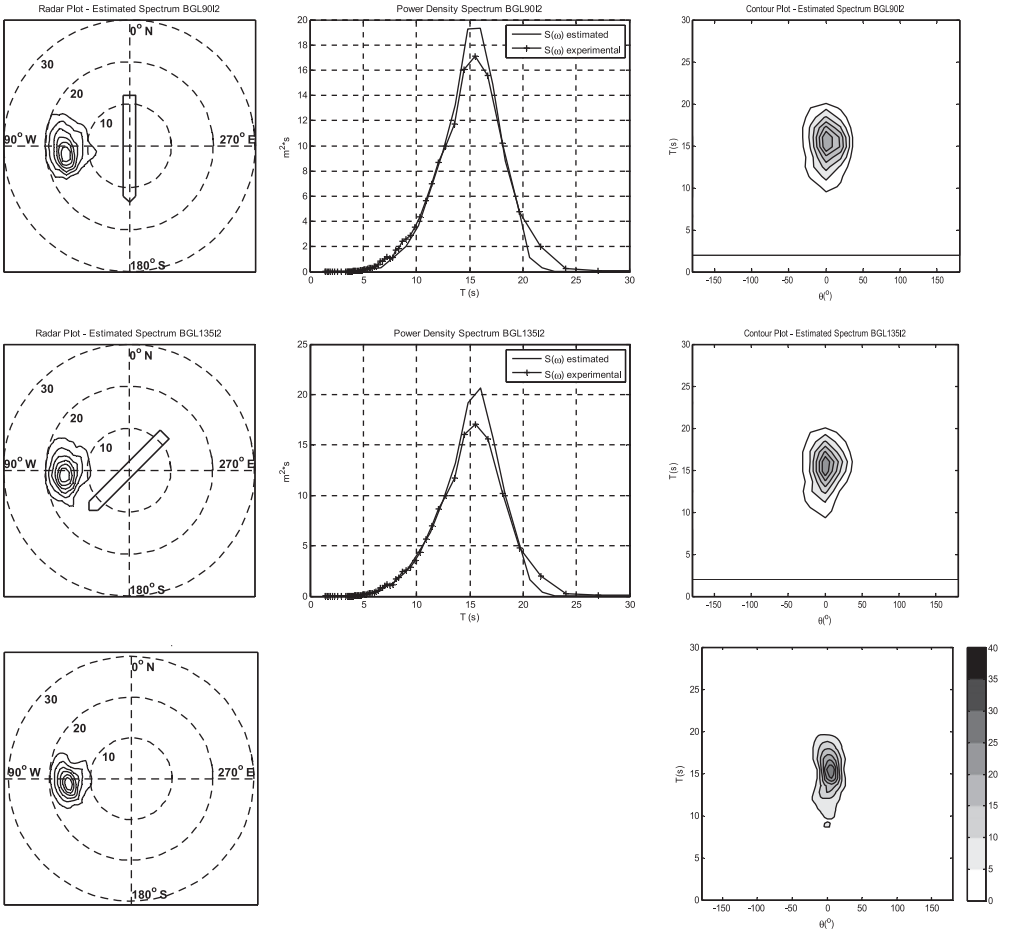


**Fig. 7.** Estimation for a 100-yr unimodal waves: (up) 90° incidence angle; (middle) 135° incidence angle; (down) Experimental Spectrum estimated by wave-probe array.

The results presented in Table 4 show that the agreement of the s-factor is satisfactory for beam-sea tests (BGL90IX), while higher discrepancies are observed concerning the 135° incidence angle. The γ-factor is quite well recovered for both sets of trials, what could indeed be anticipated by the fair agreement observed in the comparisons of the power spectra (Fig. 6).

**Table 4**
Experimental results of the Bayesian estimation – unimodal waves – spreading and peakedness factors.

| Case | Specification | | Wave-probe array | | Bayesian | |
|---|---|---|---|---|---|---|
| | $s$ | $\gamma$ | $s$ | $\gamma$ | $s$ | $\gamma$ |
| BGL90I1 | Inf. | 1.5 | 49 | 1.7 | 41 | 1.7 |
| BGL90I3 | 60 | 1.5 | 27 | 1.0 | 29 | 1.2 |
| BGL90I4 | 12 | 1.5 | 13 | 1.6 | 12 | 1.7 |
| BGL90I2 | Inf. | 1.7 | 46 | 1.8 | 35 | 1.8 |
| BGL135I1 | Inf. | 1.5 | 49 | 1.7 | 32 | 1.8 |
| BGL135I3 | 60 | 1.5 | 27 | 1.0 | 30 | 1.3 |
| BGL135I4 | 12 | 1.5 | 13 | 1.6 | 23 | 1.8 |
| BGL135I2 | Inf. | 1.7 | 46 | 1.8 | 34 | 1.7 |

**Table 5**
Experimental results of the Bayesian estimation – bimodal waves – average statistic values.

| Case | Wave-probe estimation | | | Motion-based estimation | | | Errors | | |
|---|---|---|---|---|---|---|---|---|---|
| | $H_s$ (m) | $T_p$ (s) | Dir (deg) | $H_s$ (m) | $T_p$ (s) | Dir (deg) | $H_s$ (%) | $T_p$ (%) | Dir (deg) |
| BGL120B1 | 1.62 | 11.43 | −2.0 | 1.57 | 11.33 | −5.8 | −3.4 | −0.9 | −3.7 |
| BGL120B2 | 1.93 | 7.48 | −12.4 | 1.98 | 7.83 | −5.9 | 2.5 | 4.7 | 6.5 |
| BGL120B3 | 1.22 | 5.33 | 0.4 | 1.12 | 5.50 | −0.9 | −8.0 | 3.1 | −1.3 |
| BGL120B4 | 2.14 | 11.43 | −1.3 | 2.16 | 11.33 | −4.2 | 1.3 | −0.9 | −2.9 |
| BGL120B5 | 1.59 | 12.06 | −15.0 | 1.64 | 11.33 | −10.9 | 3.4 | −6.0 | 4.1 |
| BGL150B1 | 1.62 | 11.43 | −2.0 | 1.55 | 11.33 | −6.9 | −4.5 | −0.9 | −4.9 |
| BGL150B2 | 1.93 | 7.48 | −12.4 | 1.84 | 7.83 | −16.2 | −4.7 | 4.7 | −3.8 |
| BGL150B3 | 1.22 | 5.33 | 0.4 | 1.09 | 5.50 | −4.7 | −10.4 | 3.1 | −5.1 |
| BGL150B4 | 2.14 | 11.43 | −1.3 | 2.12 | 11.33 | −6.1 | −0.7 | −0.9 | −4.8 |
| BGL150B5 | 1.59 | 12.06 | −15.0 | 1.57 | 11.33 | −17.9 | −1.1 | −6.0 | −3.0 |

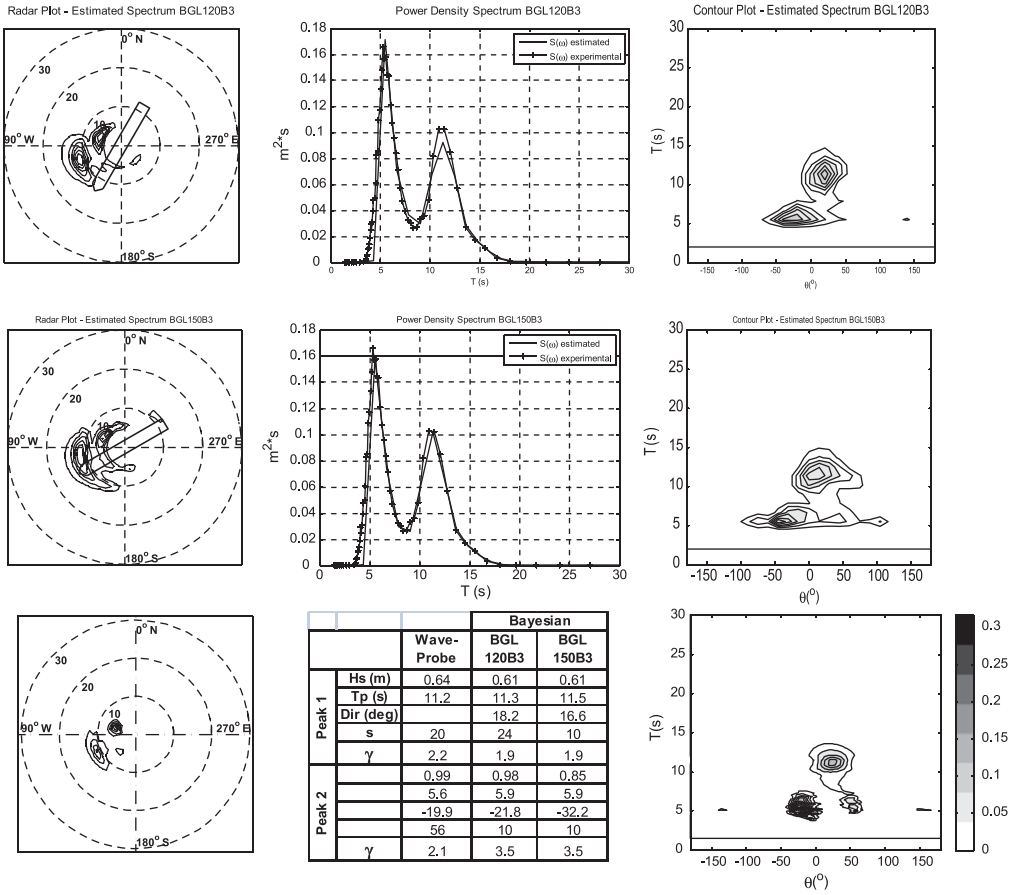


**Fig. 8.** Estimation for a BGLXXXB3 bimodal wave: (up) 120° heading angle; (middle) 150° heading angle; (down) Experimental Spectrum estimated by wave-probe array and numerical comparisons between peaks.

### 4.2. Bimodal waves

More demanding problems are posed by the tests with bimodal wave spectra, generated in the wave basin by means of the superposition of two long-crested seas. The global (average) statistics of the estimated spectra for the 5 bimodal waves are presented in the Table 5, for the two different heading angles of the model (120° and 150°). The errors are quite satisfactory, being smaller than 10.4% for $H_s$, 6% for $T_p$ and 6.5° for mean wave direction. The global statistics are important, since they define the total energy of the sea and the average direction of the individual wave fronts. However, a good wave inference device shall be able to properly define each peak in crossed-sea conditions. This can be done via motion-based estimation if both components induce significant vessel motions. The BGLXXXB3 cases illustrate such topic (Fig. 8). In this case, a mild sea with large period comes from the positive direction (related to the tank coordinate system) and the second component, with more energy and smaller period, comes from the negative direction. The peaks are clearly distinguished both in direction and frequency. The two pictures in the lower part of the figure contain the actual wave spectrum estimated by the wave-probe array. The estimations by motion-based method are quite reasonable, considering the average values (see Table 5) and the power density spectrum. Some energy filtering can be observed for components with period smaller than 5 s, which may be responsible for slightly underestimating the total wave height (8% for BGL120B3 case and 10.4% for BGL150B3).

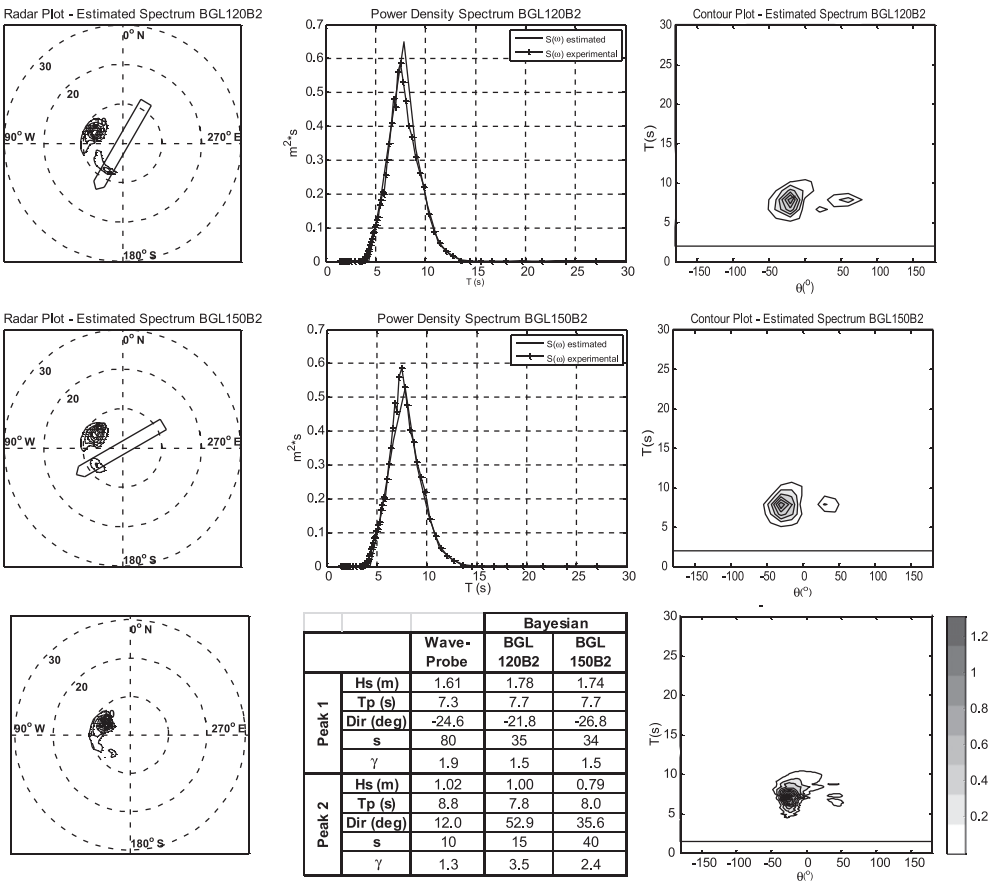


| | | Wave-Probe | Bayesian BGL 120B2 | Bayesian BGL 150B2 |
|---|---|---|---|---|
| Peak 1 | Hs (m) | 1.61 | 1.78 | 1.74 |
| | Tp (s) | 7.3 | 7.7 | 7.7 |
| | Dir (deg) | -24.6 | -21.8 | -26.8 |
| | s | 80 | 35 | 34 |
| | γ | 1.9 | 1.5 | 1.5 |
| Peak 2 | Hs (m) | 1.02 | 1.00 | 0.79 |
| | Tp (s) | 8.8 | 7.8 | 8.0 |
| | Dir (deg) | 12.0 | 52.9 | 35.6 |
| | s | 10 | 15 | 40 |
| | γ | 1.3 | 3.5 | 2.4 |

**Fig. 9.** Estimation for a BGLXXXB2 bimodal wave: (up) 120° heading angle; (middle) 150° heading angle; (down) Experimental Spectrum estimated by wave-probe array and numerical comparisons between peaks.

By the visual analysis of the estimated directional spectrum, one can verify a larger energy spreading for the peak with smaller period. The position of each peak (direction and period) is reasonable, consistent with the wave-probe estimation. In order to quantify such comparison, a 10-parameter bimodal spectrum was fitted to the estimated spectrum, and the results are exposed in the lower table (Fig. 8). Very good agreement between estimation methods is verified for the height ($H_s$) and peak period ($T_p$) of both sea components. The other parameters (direction, $s$- and $\gamma$-factors) are fairly well estimated for the low-frequency component (peak 1); since these waves induce higher amplitudes of vessel motion they can, therefore, be more accurately estimated. The high-frequency peak (peak 2 cannot be inferred with the same degree of accuracy, for the peak period (5.6 s) is very close to the cut-off period of the barge (approximately 5 s). Nevertheless, it is identified by the method and although energy is more spread than expected, the wave height remains well captured.

Similar conclusions can be drawn from the analysis of the cases BGLXXXB2 (Fig. 9). In this case, the peak with more energy (Peak 1) is very well estimated by the motion-based method, for both vessel's headings. The only parameter that presents some higher discrepancies is the s-factor (spreading). In fact, motion-based method estimates a larger spreading for the first peak, as can be inferred by the radar or contour plots. The second peak is also estimated by the motion-based approach, but larger errors are once again verified, mainly in the direction and shape factors.

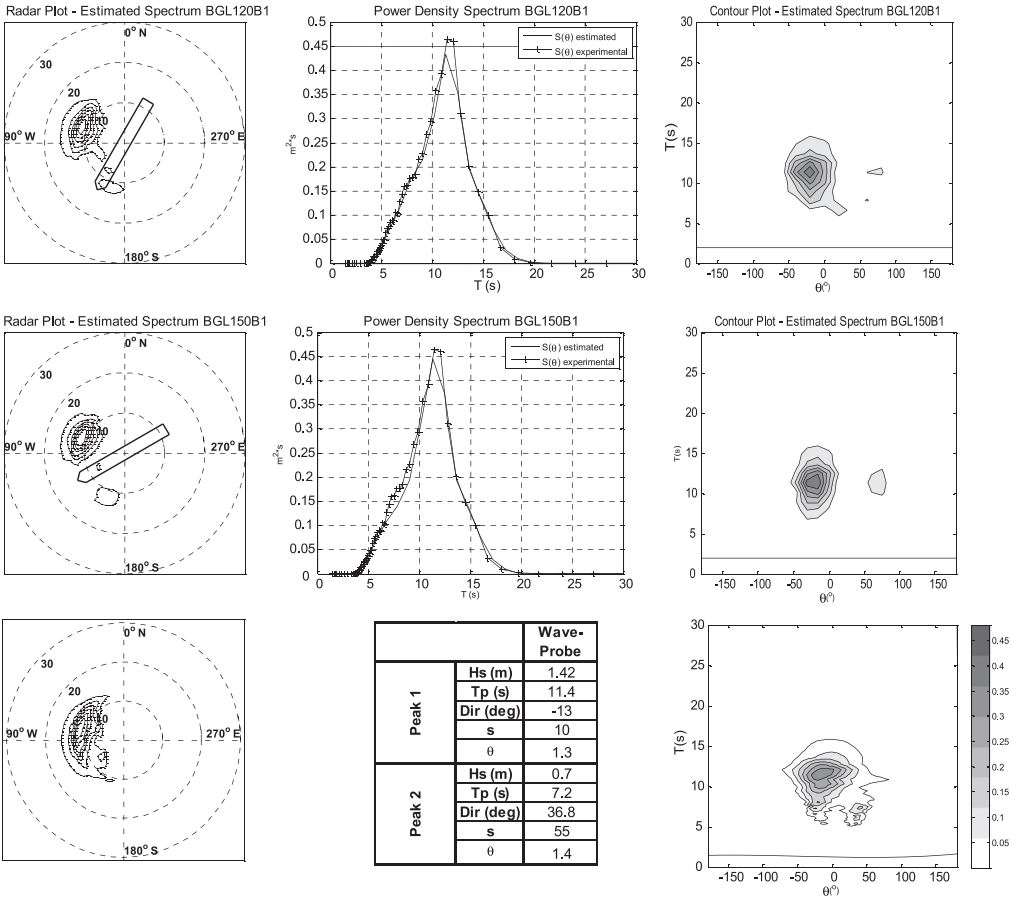


| | | Wave-Probe |
|---|---|---|
| Peak 1 | Hs (m) | 1.42 |
| | Tp (s) | 11.4 |
| | Dir (deg) | -13 |
| | s | 10 |
| | θ | 1.3 |
| Peak 2 | Hs (m) | 0.7 |
| | Tp (s) | 7.2 |
| | Dir (deg) | 36.8 |
| | s | 55 |
| | θ | 1.4 |

**Fig. 10.** Estimation for a BGLXXXB1 bimodal wave: (up) 120° heading angle; (middle) 150° heading angle; (down) Experimental Spectrum estimated by wave-probe array.

Another interesting case is represented in Fig. 10 (BGLXXXB1). In this case, the second peak cannot be clearly identified, since the $\gamma$-factors are small (1.3 and 1.4 respectively), indicating a broader frequency range (less narrow peak). There is a significant superposition of the energy spectrum of both components. The first peak evolves the second one, as can be observed by the power density spectrum. So, in this case, although the global statistics are quite well estimated by the motion-based method, the second peak (with lower period) is not clearly estimated by the method. However, a tendency to recover some of the wave energy coming from the direction of the peak 2 can be seen in the contour plots.

The cases BGLXXXB4 were supposed to emulate a bimodal-sea a state in which the two-peaks presented the same frequency and 60° angular deviation. However, the analysis of the wave-probe spectrum estimation (Fig. 11 – lower graphics) indicates that the wave-generator was not able to create the two-peaks with a clear distinction. The result is a spread unimodal wave spectrum, covering the angular range involving the two specified peaks. A very good estimate of such spread spectrum is obtained with the motion-based method, mainly for the 120° heading.

Finally, the tests BGLXXXB5 (Fig. 12) present a bimodal sea state with both components coming from the same direction, but with different peak periods. In this case, the peak with lower period can be identified both in the power density spectrum and in the directional spectrum. The motion-based

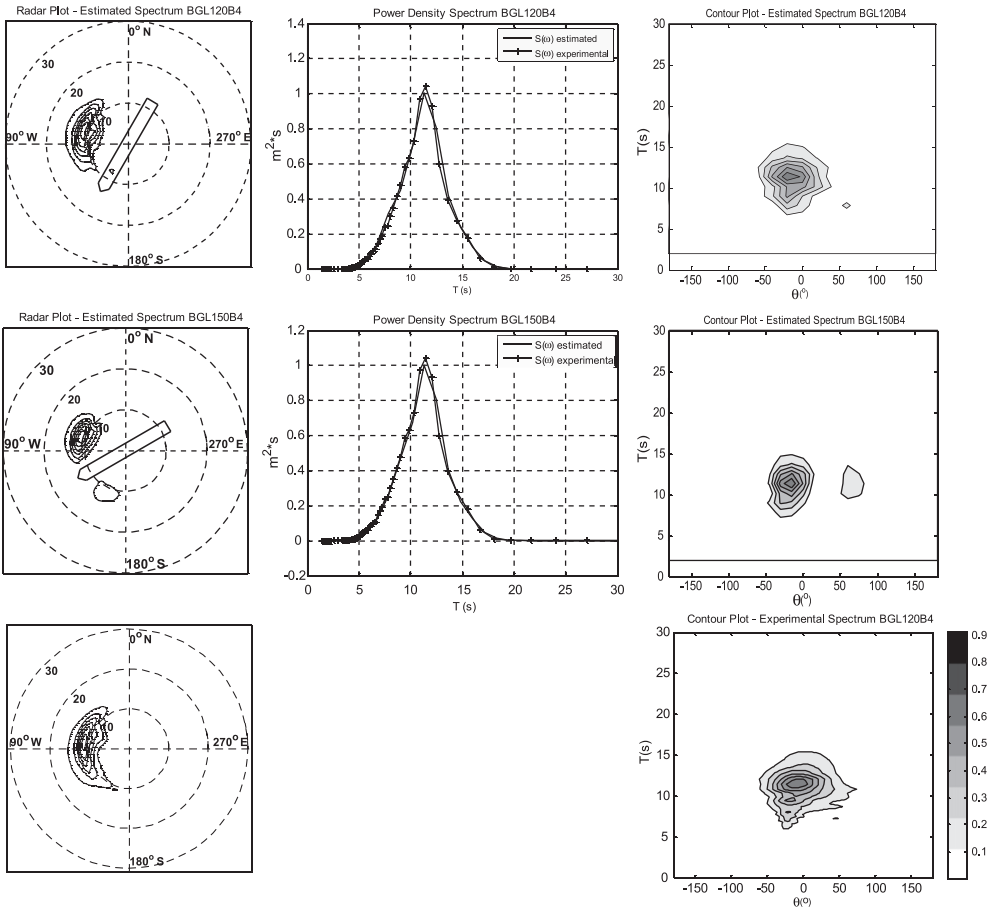


**Fig. 11.** Estimation for a BGLXXXB4 bimodal wave: (up) 120° heading angle; (middle) 150° heading angle; (down) Experimental Spectrum estimated by wave-probe array.

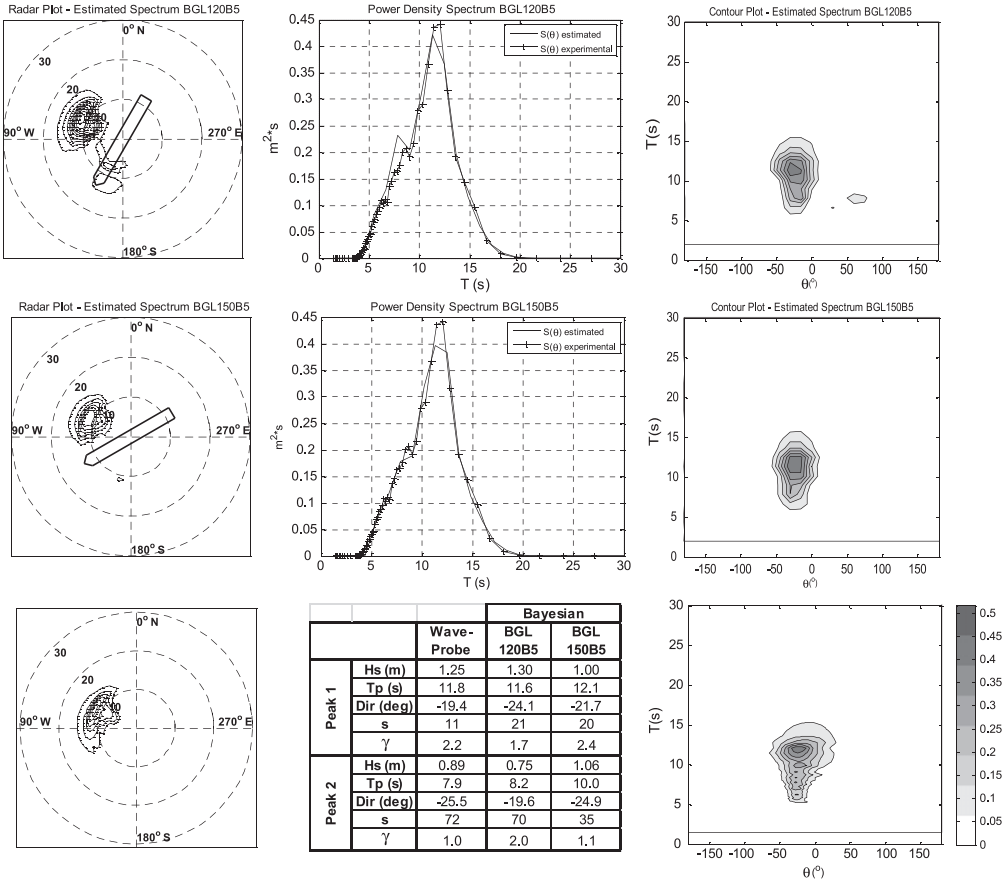


| | | Wave-Probe | Bayesian BGL 120B5 | Bayesian BGL 150B5 |
|---|---|---|---|---|
| Peak 1 | Hs (m) | 1.25 | 1.30 | 1.00 |
| | Tp (s) | 11.8 | 11.6 | 12.1 |
| | Dir (deg) | -19.4 | -24.1 | -21.7 |
| | s | 11 | 21 | 20 |
| | γ | 2.2 | 1.7 | 2.4 |
| Peak 2 | Hs (m) | 0.89 | 0.75 | 1.06 |
| | Tp (s) | 7.9 | 8.2 | 10.0 |
| | Dir (deg) | -25.5 | -19.6 | -24.9 |
| | s | 72 | 70 | 35 |
| | γ | 1.0 | 2.0 | 1.1 |

**Fig. 12.** Estimation for a BGLXXXB5 bimodal wave : (up) 120° heading angle; (middle) 150° heading angle; (down) Experimental Spectrum estimated by wave-probe array and numerical comparisons between peaks.

method could actually estimate this spectrum, as can be assured by the table containing the 10-parameters (also estimated by a function-fitting algorithm). For the 120° heading, the results are even closer to the wave-probe estimation due to the beam-sea condition in this case (the advantages of estimating a beam-sea wave was also verified in the analysis of unimodal spectra).

In summary, the analysis of the different bimodal tests indicates that the average statistics of all bimodal waves were accurately estimated. Furthermore, the identification of the crosses-sea components was possible for all cases provided that the overlap in their energy density was not substantial. In fact, taking into account the difficulties associated to identifying the peak-parameters in a bimodal sea state by measuring the vessel's motions, a certain level of error may be considered acceptable, particularly regarding the shape parameters (s- and γ-factors).

## 5. Conclusion

The accuracy of a motion-based inference method for predicting the directional wave spectrum was tested by means of model tests performed in a wave basin. The model of the Petrobras' BGL1 crane-barge was employed in tests with different sea conditions. The wave statistics were representative of Campos Basin conditions and the tests included long-crested seas, unimodal seas with different directional spreading and also crossed-sea conditions (the latter generated in the basin by the

combination of two different long-crested components). The wave estimations (statistics, power spectra and directional spectra) obtained from the measured motions of the model were compared to those derived from the measurements of an array of eight wave probes, which was employed for wave calibration.

Results indicated an overall good agreement between motion-based and probes-based inference for both, unimodal and bimodal sea conditions. Regarding the unimodal (single-peaked) conditions, the errors obtained from motion-based inference were very small for all tests. Not only could the mean statistics be well reproduced, but also the spreading and peakedness factors were captured with quite reasonable accuracy.

Comparisons performed with the crossed-sea spectra demonstrated that, provided the energy overlap of the wave components is narrow, both can be reasonably identified in the motion-based inference. Obviously, the accuracy in the estimation of each component also depends on the level of motions imposed by each one of them, as illustrated by the results. Nonetheless, the method was able to identify with reasonable accuracy even wave components with very low peak periods, around 5 s. As a trend, it was verified that the global (average) wave statistics were well reproduced, especially concerning the mean wave height and period. Discrepancies were generally larger for the mean directions and shape parameters of the individual sea components, although even for these parameters the results may be considered quite acceptable, considering the difficulties that are inherent to this kind of estimation.

The inference method presented in this paper is currently being employed in a field campaign on-board one of the Petrobras FPSOs, aiming at an additional validation in real-scale. Tests will also be performed on-board the BGL1 barge and the results shall be presented in the near future.

## Acknowledgments

Authors gratefully acknowledge Petrobras for supporting the research project conducted at the University of São Paulo and providing the funds that made this experimental campaign possible. First and second authors acknowledge CNPq, the Brazilian National Research Council, for their respective research-grants.

## References

[1] Hua J, Palmquist M. Wave estimation through ship motion measurement. Naval Arch., Dept. of Vehicle Eng., Royal Institute of Technology; 1994. Technical Report.
[2] Iseki T, Ohtsu K. Bayesian estimation of directional wave spectra based on ship motions. Control Engineering Practice 2000;8:215–9.
[3] Iseki, T. Extended Bayesian estimation of directional wave Spectra. Proc. of the 23rd Int. Conf. on Offshore Mech. And Arctic Eng. (OMAE2004), ASME, June 20–25, Vancouver, Canada, paper OMAE2004–51609; 2004.
[4] Pascoal R, Guedes Sørensen C, Sorensen AJ. Ocean wave spectral estimation using vessel wave frequency motions. Proc. of the 24th Int. Conf. on Offshore Mech. and Artic Eng. (OMAE2005), ASME, June 12–17, Halkidiki, Greece, paper OMAE2005-67584; 2005.
[5] Nielsen UD. Estimation of directional wave spectra from measured ship responses. Ph.D. thesis. Section of Coastal, Maritime and Structural Engineering, Department of Mechanical Engineering, Technical University of Denmark; 2005.
[6] Nielsen UD. Estimations of on-site directional wave spectra from measured ship responses. Marine Structures 2006;19: 33–69.
[7] Nielsen UD. Response-based estimation of sea state parameters – influence of filtering. Ocean Engineering 2007;34: 1797–810.
[8] Nielsen UD. Introducing two hyperparameters in Bayesian estimation of wave spectra. Probabilistic Engineering Mechanics 2008;23:84–94.
[9] Nielsen UD, Iseki T. Estimation of sea state parameters from measured ship responses – the Bayesian approach with fixed hyperparameters. Proc. of the 29th Int. Conf. on Offshore Mech. And Artic Eng. (OMAE2010), ASME, June 6-11, Shanghai, China, paper OMAE2010–20099; 2010.
[10] Tannuri EA, Sparano JV, Simos AN, Da Cruz JJ. Estimating directional wave spectrum based on stationary ship motion measurements. Applied Ocean Research 2004;25:243–61.
[11] Simos AN, Sparano JV, Tannuri EA, Matos VLF. Directional wave spectrum estimation based on a vessel 1st order motions: field results; 2007. The 17th International Offshore and Polar Engineering Conference, ISOPE2007, Lisbon, Portugal.
[12] Simos AN, Tannuri EA, Sparano JV, Matos VLF. Estimating wave spectra from the motions of moored vessels: experimental validation. Applied Ocean Research 2010;32:191–208.
[13] Akaike H. Likelihood and Bayes procedure. In: Bernardo JM, de Groot MH, Lindley DU, Smith AFM, editors. Bayesian statistics. Valencia: University Press; 1980. p. 143–66.

[14] Stansberg CT. On the fourier series decomposition of directional wave spectra; 1998. Proc.. of the 8th Int. Off. and Polar Eng. Conf. ISOPE98, Montréal, Canadá, May 24–29, pp. 227–233.
[15] Tannuri EA, Mello PC, Sales Junior JS, Simos AN, Matos VLF. Estimation of directional wave spectrum using a wave-probe array. Proc. of 3rd Int. Workshop on Applied Offshore Hydrodynamics, Rio de Janeiro, Brazil; 2007.
[16] Goda Y. Random seas and design of marine strucutres, advanced series on ocean eng. 2nd ed., vol. 15. World Scientific; 2000.
[17] WAMIT. Wave analysis program: reference manual. WAMIT, Inc; 2000.